Available online at www.sciencedirect.com
SCIENCE DIRECT®
Estuarine, Coastal and Shelf Science 63 (2005) 683–700
ESTUARINE COASTAL AND SHELF SCIENCE
www.elsevier.com/locate/ECSS

Fluxes and sources of suspended organic matter in an estuarine turbidity maximum region during low discharge conditions

Miguel A. Goni[a,*], Mary W. Cathey[a], Yong H. Kim[a], George Voulgaris[b]

[a]Department of Geological Sciences, University of South Carolina, Columbia, SC 29208, USA
[b]Department of Geological Sciences, Marine Science Program, University of South Carolina, Columbia, SC 29208, USA

Received 9 February 2004; accepted 24 January 2005

Abstract

Water column concentrations of total suspended solids (TSS), particulate organic carbon (POC) and particulate nitrogen (PN) were measured at three different depths in four different locations bracketing the estuarine turbidity maximum (ETM) along the main channel of a temperate riverine estuary (Winyah Bay, South Carolina, USA). Measurements were carried out over full tidal cycle (over 24 h). Salinity, temperature, current magnitude and direction were also monitored at the same time throughout the water column. Tidally averaged net fluxes of salt, TSS, POC and PN were calculated by combining the current measurements with the concentration data. Under the extreme low river discharge conditions that characterized the study period, net landward fluxes of salt were measured in the lower part of the study area, suggesting that the landward transport through the main channel of the estuary was probably balanced by export out through the sides. In contrast, the net fluxes of salt in the upper reaches of the study area were near zero, indicating a closed salt balance in this part of the estuary. In contrast to salt, the net fluxes of TSS, POC and PN in the deeper parts of the water column were consistently landward at all four sites in Winyah Bay indicating the non-conservative behavior of particulate components and their active transport up the estuary in the region around the ETM.

The carbon contents (%POC), carbon:nitrogen ratios (org[C:N]a) and stable carbon isotopic compositions ($\delta^{13}C_{POC}$) of the suspended particles varied significantly with depth, location and tidal stage. Tidally averaged compositions showed a significant increase up the estuary in the %POC and org[C:N]a values of suspended particles consistent with the preferential landward transport of carbon-rich particles with higher vascular plant debris content. The combination of tidal resuspension and flood-dominated flow appeared to be responsible for the hydrodynamic sorting of particles along the estuary that resulted in denser, organic-poor particles being transported landward less efficiently. The elemental and isotopic compositions indicated that vascular C_3 plants and estuarine algae were the major sources of the particulate organic matter of all the samples, without any significant contributions from salt marsh C_4 vegetation (*Spartina alterniflora*) and/or marine phytoplankton.

Keywords: estuarine carbon fluxes; organic matter sources; carbon:nitrogen ratios; stable carbon isotopes; Winyah Bay

1. Introduction

Continental margins are key sites for the biogeochemical cycling of organic carbon in the ocean. As transitional environments within the continental margins, estuaries play an important role in regulating the flux of carbon and associated materials between the land and the ocean. For example, estuaries receive organic matter (OM) from multiple sources that include vascular plants, soil organic matter, and the remains of algae, and micro-organisms (e.g., Cifuentes et al., 1988; Canuel et al., 1995; Yunker et al., 1995; Cifuentes and Eldridge, 1998; Hopkinson et al., 1998; Raymond and Bauer, 2000; Leithold and

* Corresponding author. Department of Geological Sciences, Earth Water Sciences Building 302, 701 Sumter Street, University of South Carolina, Columbia, SC 29208, USA.
E-mail address: goni@geol.sc.edu (M.A. Goni).

0272-7714/$ - see front matter © 2005 Elsevier Ltd. All rights reserved.
doi:10.1016/j.ecss.2005.01.012

Blair, 2001; Canuel, 2001; Harvey and Mannino, 2001; Masiello and Druffel, 2001; Shi et al., 2001). Once they enter estuaries, the fates of these various OM pools largely depend on their inherent properties (e.g. reactivity) and their overall residence time in these systems.

Estuaries are extremely dynamic environments that respond to physical forces on time scales ranging from semi-diurnal (tidal) to fortnightly (spring vs. neap tides), seasonal (i.e., river discharge) and multi-year (i.e., El Niño–La Niña cycles). The combined action of these processes control sediment mobilization, transport, and deposition (e.g., Schubel, 1968; Schubel and Pritchard, 1972; Geyer, 1993; Friedrichs et al., 1998; Chant and Stoner, 2001). Hence, variations in tidal conditions and river discharge, as well as stochastic events such as large storms, have the ability to control the residence time of particles and OM, affecting important reactions such as the flocculation, solubilization, respiration, and burial of carbon.

One of the salient features of estuaries is the estuarine turbidity maximum (ETM). Formation of the ETM is typically attributed to gravitational circulation, tidal asymmetries and stratification (e.g., Allen et al., 1980; Geyer, 1993; Friedrichs et al., 2000; Chant and Stoner, 2001). The processes occurring in the ETM impart an additional fundamental control on the residence time and cycling of different OM pools. For example, the periodic resuspension of particles at the ETM may facilitate the oxidation of otherwise recalcitrant particulate OM (POM) fractions by recharging the metal-oxide phases due to repeated exposure to oxygenated water (Aller, 1994, 1998). Transformations of POM and dissolved organic matter (DOM) due to sorption/desorption processes potentially play a large role in the behavior and fate of organic carbon in estuaries (Ertel et al., 1991; Fisher et al., 1998; Zhang et al., 1998; Murrell and Hollibaugh, 2000; Abril et al., 2002). In addition, resuspension can lead to a significant hydrodynamic sorting of particles based on their differential density and settling velocities. On the other hand, resuspension events within the ETM may facilitate the release of previously deposited OM via desorption. Overall, because different OM pools are distinctly distributed among size and density classes, all these processes can directly affect the biogeochemical cycles of estuarine ecosystems.

Given the complexity of the above-described processes, this study presents field data that aim at elucidating the role that physical processes have on the fate of POM in the vicinity of an ETM from a partially mixed estuary (Winyah Bay, SC, USA). The specific objectives of the study are to determine the relationship between TSS and POM around the ETM at different stages of the tidal cycle, estimate net tidally averaged fluxes of TSS and POM and identify POM sources during the low freshwater discharge conditions encountered during the sampling period. Additional data from periods of high discharge conditions are planned to investigate TSS and POM transport and cycling in this estuarine system under different hydrographic regimes.

2. Methods and materials

2.1. Study area

Winyah Bay, one of the largest estuaries on eastern coast of the US, is located adjacent to the port city of Georgetown, South Carolina (Fig. 1). Its drainage basin covers an area of 46,736 km^2 and extends to the Blue Ridge Mountains of North Carolina. The bay receives freshwater primarily from the Pee Dee, Black, Waccamaw, and Sampit Rivers, with the Pee Dee contributing approximately 90% of the total discharge. The latter is also the primary source of sediment to Winyah Bay and has a drainage basin that extends over an area of 41,451 km^2. Forestry and agriculture are the dominant activities in the drainage basin, although conversion of these lands for urban and industrial use is currently underway. The Sampit and Waccamaw Rivers, which are black water rivers that drain the low-lying topography of the coastal plain, contribute a relatively small fraction (<10%) of the total sediment load to Winyah Bay. The bay has a surface area of 155.4 km^2 and a mean depth of 4.2 m (Blood and Vernberg, 1992).

In order to accommodate large ship traffic, a 29 km-long channel is dredged to a depth of 8.2 m every 12–18 months (Blood and Vernberg, 1992; USACOE, 1997). The central part of the estuary includes an additional natural channel of a mean water depth of 5 m located to the west of main navigation channel that contributes to a residual circulation pattern (see Kim and Voulgaris, submitted for publication). The tides are semi-diurnal with neap and spring tidal ranges of 1 and 1.5 m, respectively, near the mouth of the estuary increasing by up to 20% in the upper reaches of the estuary. Winyah Bay is a partially mixed, type B estuary according to the Pritchard (1967) classification scheme (Blood and Vernberg, 1992; Ramsey, 2000; Kim and Voulgaris, submitted for publication) with a complex morphology.

2.2. Data collection and analysis

Data were collected during the period October 4–5, 2001 at four locations (hereafter referred to as stations WB5, WB6, WB7 and WB8, respectively) in the upper reaches of Winyah Bay (Fig. 1). The sampling stations bracketed the position of the ETM at the low discharge conditions that characterized our data collection period. The two upper stations, WB8 and WB7, are located within the upper reaches of the estuary (single channel) whereas the other two (WB6 and WB5) are located in the regions of Winyah Bay that is characterized by

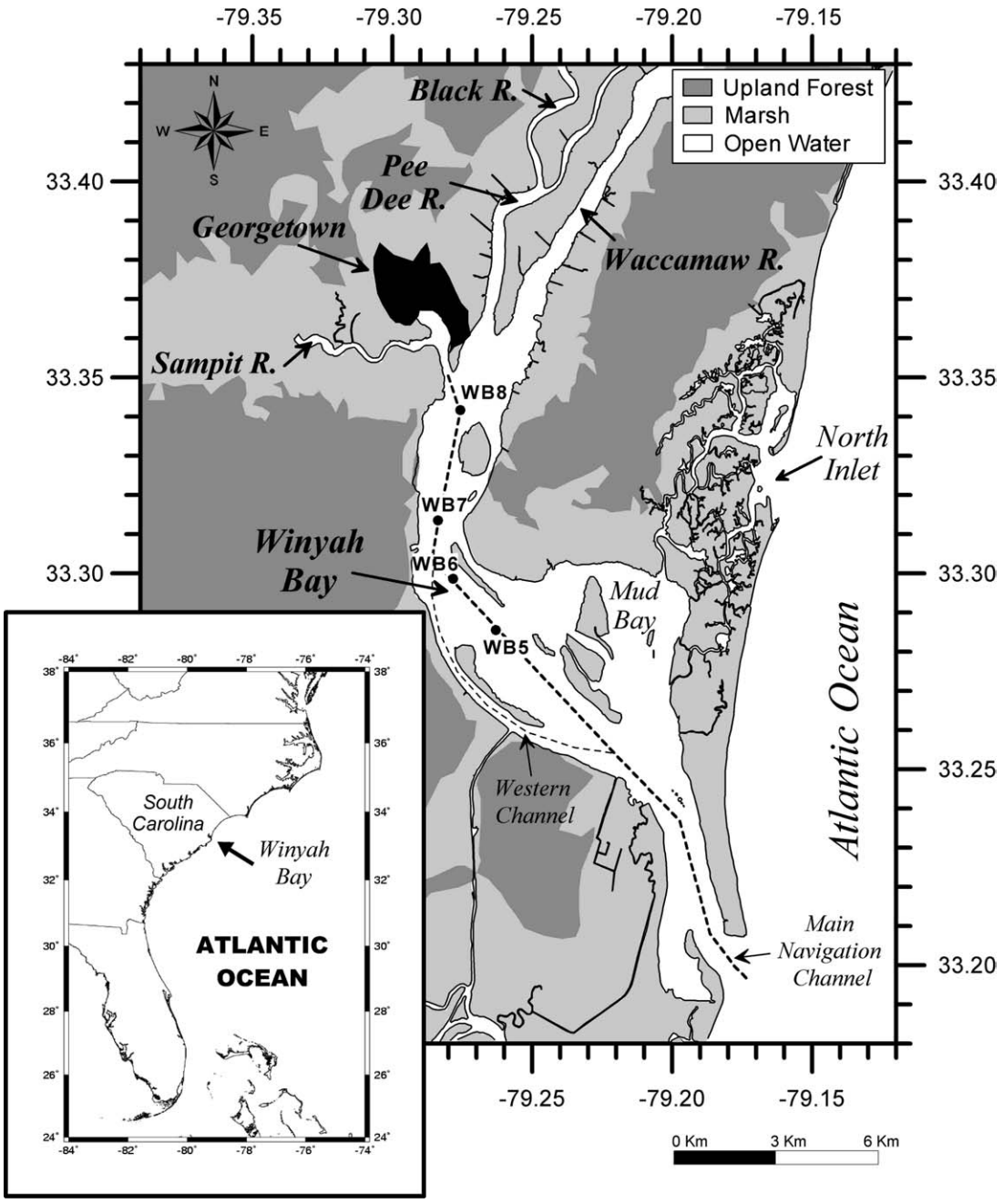

Fig. 1. Map of Winyah Bay (South Carolina) with sampling locations and codes. The locations of the main navigation channel and the western channel are indicated in the map.

a dual channel morphology (Fig. 1). The size of the research vessel used (NOAA R/V Ferrel) limited sample and data collection to the main navigational channel. During sampling stations were occupied sequentially from WB5 to WB8, with the vessel returning to WB5 in order to repeat the sampling sequence. This approach provided a temporal coverage at each of the four stations that varied between 2 and 3 h and was sufficient to resolve tidal variability.

The vertical distribution of current speed and direction were measured at each station and a hydrocast was conducted to profile the entire water column and collect water samples at three depths (near surface, mid-depth and near bottom). During each hydrocast, continuous profiles of depth, salinity, and temperature were measured using a CTD. During the upcast, water samples from three different depths were collected using a submersible pump, which was attached to the CTD. Water samples were pumped from depth via a hose into acid-washed, sample-rinsed opaque Nalgene bottles. Upon collection, water samples were filtered for geochemical measurements of suspended particles.

2.2.1. Hydrography and current measurements

Salinity, temperature and depth were measured using an Ocean Sensors 200 CTD. Data were collected at approximately 1 Hz rate resulting in a vertical resolution of approximately 2.5 cm. These data where subsequently depth averaged to 25 cm bin averages to coincide with the vertical resolution of the current measurements (see below). The vertical structure of the currents at each station was measured using a ship-mounted downward-looking Acoustic Doppler Current Profiler (ADCP, 1200 kHz Workhorse, RD Instruments) equipped with a bottom tracking capability. The three components of the flow were recorded continuously at 25 cm bin intervals while the vessel was on station and were subsequently time-averaged for the period of the cast and water sampling operations, which varied between 2 and 10 min. The horizontal current velocities were collected into the geographical orthogonal coordinate system (i.e., north and east current components) and later converted into a local orthogonal coordinate system with the X-axis being aligned with the direction of the main channel (along-channel component, positive values indicating flood direction).

2.2.2. Suspended particle analyses

Suspended particulate matter was isolated immediately after collection by filtering variable volumes of water (30–300 ml) under vacuum in the ship's laboratory. Pre-weighed and pre-combusted 47-mm diameter GF/F filters (0.7 μm pore size) were used. Filters were stored at −20 °C until returned to the laboratory on the main land, where they were oven-dried at 50 °C for at least 48 h and reweighed. Total suspended sediment (TSS) concentration was determined by the weight difference divided by the volume of water filtered.

Using the approach described for TSS, known volumes (4–40 ml) of water were filtered through pre-combusted 13-mm diameter GF/F filters (1.0 μm nominal pore size). Four filters were collected from each water sample in order to carry out elemental and stable carbon isotope analyses. Filters were stored at −20 °C, until returned to the laboratory, where they were dried at 50 °C for at least 48 h. Dried filters were loaded into silver boats, placed in a dessicator and exposed to concentrated HCl vapors under vacuum for 36–48 h in order to remove carbonates (Hedges and Stern, 1984). Samples were vented for 24 h, and dried at 50 °C for at least 48 h prior to analysis.

POC and PN concentrations were determined by high temperature combustion on a Thermo Quest EA2500 Elemental Analyzer. The combustion and reduction oven temperatures were 1020 °C and 640 °C, respectively, and helium was used as the carrier gas. POC and PN concentrations were calculated based on calibration curves generated daily from sets of cystine standards. Pre-combusted blank filters were also analyzed to determine OC and N content of the filter itself. Samples and blanks were randomly run in triplicate to determine analytical variability.

2.2.3. Stable carbon isotopic analysis

Prior to measuring stable carbon isotopic compositions of POC samples ($\delta^{13}C_{POC}$), filters were acidified in the same manner as for elemental analyses (see Section 2.2.3). Stable carbon isotopic analyses were performed on a ThermoQuest EA interfaced with a Finnigan Mat Delta Plus-XLS by a Conflo-III system. Three standards with a range of isotopic values were used to generate an isotopic calibration curve (sucrose, −10.47‰; cystine, −16.65‰; and polystyrene foil, −31.77‰). In order to account for the $\delta^{13}C$ of the filter itself, blank filters were also analyzed. $\delta^{13}C_{POC}$ values were determined by mass balance, using the following equation:

$$\delta^{13}C_{POC} = \left[\frac{\delta^{13}C_s - (\delta^{13}C_b \times f_b)}{f_{POC}}\right] \quad (1)$$

where $\delta^{13}C_s$ represents the isotopic composition of the whole filter sample as determined from the instrument, $\delta^{13}C_b$ is the isotopic composition of blank filters, f_b is the fraction of OC in the sample associated with the blank filter and f_{POC} is the fraction of the OC in the filtered sample that is derived from suspended organic matter (i.e., $f_b + f_{POC} = 1$). The OC contents of the blanks and samples were determined from the elemental analyses.

2.3. Statistical treatment of data

The propagation of error associated with parameters, such as the carbon:nitrogen and POC:TSS ratios, were calculated using (Taylor, 1982):

$$\sigma_q = \left[\left(\frac{\partial q}{\partial x}\sigma_x\right)^2 + \left(\frac{\partial q}{\partial y}\sigma_y\right)^2\right]^{1/2} \quad (2)$$

where σ_q is the standard deviation of the ratio of two independent variables x and y with standard deviations σ_x and σ_y, respectively. The variability associated with tidally averaged parameters was evaluated using standard errors (s.e. $= \sigma_x/n^{1/2}$, where n is the number of discrete samples). Student t-tests were used to assess differences among tidally averaged sample means. All results are reported as statistically significant at the 95% confidence interval ($p < 0.05$) unless otherwise noted.

3. Results

3.1. Hydrography

Freshwater discharge by rivers into Winyah Bay during the period of this study was extremely low as

a result of the extensive draught conditions that occurred in the southeastern U.S. from 1999 to 2002. In 2001, the Pee Dee River, which typically contributes approximately 90% of the total freshwater flow, had the lowest average discharge in the past 50 years for the month of October (28 $m^3 s^{-1}$). The draught throughout all of 2001 meant that the combined annual river discharge of the Waccamaw, Black and Pee Dee Rivers during 2001 was at record low levels (193 $m^3 s^{-1}$) below the 50-year mean (241 $m^3 s^{-1}$). In fact, the combined river discharge during 2001 was the fourth lowest average annual discharge in the past 50 years (U.S. Geological Survey; station #s 2131000, 2136000 and 2110500; http://waterdata.usgs.gov/nwis/sw).

The hydrographic data from specific depths at each station are summarized in Table 1. The temporal and vertical trends of the along-channel current velocity for the two tidal periods examined in this study are shown in Fig. 2. The currents showed marked variability as a function of tidal stage. Maximum ebb velocities ranged from 60 cm s^{-1} at WB8 to 100 cm s^{-1} at WB7. Ebb velocities were highest in the mid to upper portion of the water column at every station and tended to decrease with depth. The two upper bay stations proximal to the riverine input (WB7, WB8) showed the highest ebb velocities possibly due to the narrower width of the estuary at these locations. Maximum flood velocities occurred in the mid to lower portion of the water column. Flood velocities reached values over 100 cm s^{-1} at the two lower bay stations (WB5 and WB6), while velocities in the two upper bay stations (WB7 and WB8) reached 80–90 cm s^{-1}. The observed vertical structure of the current is typical of the estuarine environment with increased velocities near the surface during the ebb, when tidal flow and freshwater are flowing the same direction and increased velocities near the mid-water level during the flood, when freshwater flow near the surface opposes the tidal component of the flow. The flow reduction near the bed is due to bottom friction.

The temporal and spatial trends in salinity for the same period as the current measurements are shown in Fig. 3. Temperature was found to be relatively constant throughout the water column (not shown here) indicating that salinity controls water density variation in the study area. Salinity during ebb tide ranged from 8, at the surface in the most landward station (WB8) to 30 near the bed at WB5 (see Fig. 3). Salinity during flood tide ranged from 10 at the surface in WB8 to 28 near the bed at WB5, indicating partially mixed conditions. Surface waters remained relatively saline at the seaward-most station (WB5) due to extremely low river discharge that characterized the study period.

3.2. Suspended particle compositions

The compositions of the water and particle samples collected with the pumping system at three depths in each of the four Winyah Bay stations are presented in Table 1. Surface samples correspond to a depth of about 2 m, mid-water (mid) samples were collected from a depth of ca. 5 m and deep samples were collected from ca. 1 m above the bottom. Hereafter, we refer to each of these samples by their station number (i.e., WB5, WB6, WB7 and WB8) and water column location (surface, mid, deep). On average, eight samples from each depth and location were collected over two complete tidal cycles yielding a temporal resolution of approximately 3 h.

3.2.1. Total suspended sediment concentrations

TSS concentrations varied over two orders of magnitude, ranging from 50 mg L^{-1} at WB8 surface to 400 mg L^{-1} at WB7 deep (Table 1). Fig. 4 illustrates the variability and average in TSS with depth and tidal stage at each of the four stations. Overall, TSS concentrations in the surface waters exhibited no clear trends with current magnitude and direction over the tidal cycle. For example, at WB7 surface, TSS concentrations ranged from 50 to 100 mg L^{-1} while current speeds varied from -90 cm s^{-1} at maximum ebb to $+79$ cm s^{-1} at maximum flood. In some cases, TSS concentrations in the mid and deep samples showed slight trends with current magnitude and direction, so that the highest TSS values were consistently measured during peak flood (Table 1; Fig. 4). Although the statistical significance of these trends was not great ($0.3 < r^2 < 0.4$), the positive correlations between flooding current and TSS concentration at WB7 and WB8 are indicative of local sediment resuspension. The lack of stronger correlations between TSS and current magnitude could be interpreted as the effect of strong horizontal or vertical (settling) sediment advection. TSS concentrations were also poorly correlated with salinity ($0.0 < r^2 < 0.3$) for almost all stations (plots not shown). The major exception was WB8 surface, in which salinity and TSS concentrations were significantly correlated ($y = 7.78x - 14.3$; $r^2 = 0.70$; $p = 0.009$). Such poor correlation is consistent with the non-conservative mixing behavior of TSS in this part of the estuary.

In general, tidally averaged TSS concentrations (TSS*) were highest in the lower portion of the estuary, decreasing towards the upper portion of the estuary (Fig. 5a). For example, TSS* concentrations at all three depths were significantly higher in WB5 than in the other stations. Typically, the WB7 and WB8 stations displayed the lowest TSS* concentrations at each of the respective depths. The major exception was the elevated TSS* concentrations (195 mg L^{-1}) measured at WB7 deep, which coincided with the location of the ETM under the conditions encountered during sampling. At each station, TSS* concentrations increased significantly with depth, with the most marked increase observed at

Table 1
Hydrographic and geochemical data for samples

	Cast	Jul Date	Depth (m)	Salinity (psu)	Current (cm sec^{-1})	TSS (mg L^{-1})	POC (mg L^{-1})	PN (mg L^{-1})	$\delta^{13}C$ (per mil)
WB5 surface	34	278.06735	2.14	11.12	75.21	125.2	1.26	0.118	–27.3
	38	278.21145	3.93	24.08	–24.69	98.4	0.97	0.084	–29.5
	43	278.37410	2.60	15.85	–23.19	96.0	1.68	0.144	–27.8
	47	278.51837	1.82	18.64	82.37	104.4	1.40	0.190	–27.4
	51	278.67010	2.34	23.29	12.96	120.4	1.31	0.214	–27.3
	55	278.81042	1.49	21.18	–84.28	240.8	1.49	0.122	–26.3
	59	278.98021	3.12	17.14	34.36	112.8	1.41	0.123	–26.6
	63	279.10690	1.66	20.94	33.89	122.7	1.14	0.081	–27.1
		Average	*2.39*	*19.03*	*13.33*	*127.6*	*1.33*	*0.13*	*–27.3*
		Std. Error	*0.29*	*1.51*	*19.72*	*16.6*	*0.08*	*0.02*	*0.34*
WB5 mid	34	278.06735	6.16	11.14	72.01	158.6	2.19	0.203	–26.9
	38	278.21145	6.76	24.96	–9.17	101.0	1.15	0.135	–28.1
	43	278.37410	5.10	20.13	–33.91	112.2	1.37	0.160	–27.9
	47	278.51837	5.43	21.05	75.74	153.8	3.25	0.405	–26.7
	51	278.67010	4.49	27.21	45.24	212.8	1.06	0.112	–26.7
	55	278.81042	2.83	21.78	–69.64	190.2	1.68	0.140	–27.4
	59	278.98021	5.28	17.65	36.74	106.6	1.07	0.104	–27.2
	63	279.10690	4.16	23.61	69.56	165.4	1.93	0.149	–26.4
		Average	*5.03*	*20.94*	*23.32*	*150.1*	*1.71*	*0.18*	*–27.1*
		Std. Error	*0.43*	*1.75*	*19.31*	*14.4*	*0.26*	*0.03*	*0.22*
WB5 deep	34	278.06735	8.91	10.96	59.31	181.3	3.09	0.209	–26.6
	38	278.21145	7.95	25.15	–7.07	105.2	0.91	0.100	–28.1
	43	278.37410	7.40	22.06	–22.74	127.2	2.11	0.171	–27.1
	47	278.51837	6.54	21.08	75.82	163.7	3.23	0.411	–28.3
	51	278.67010	6.94	27.84	46.63	227.1	1.31	0.138	–26.9
	55	278.81042	7.77	29.96	–27.15	229.8	1.45	0.107	nd
	59	278.98021	6.66	19.33	34.38	153.7	1.34	0.117	nd
	63	279.10690	7.71	23.62	55.67	157.9	2.66	0.192	–26.6
		Average	*7.49*	*22.50*	*26.86*	*168.2*	*2.01*	*0.18*	*–27.2*
		Std. Error	*0.28*	*2.06*	*14.18*	*15.5*	*0.32*	*0.04*	*0.30*
WB6 surface	30	277.93727	1.84	10.74	9.66	79.7	1.11	0.108	–29.2
	35	278.09740	1.83	10.69	54.00	119.2	1.24	0.133	nd
	39	278.24064	1.92	19.91	–62.17	91.2	1.28	0.135	–28.3
	44	278.39914	2.27	15.33	–13.78	87.3	1.80	0.159	–28.5
	48	278.53879	2.07	17.01	105.29	93.4	1.00	0.128	–27.0
	52	278.69892	1.52	21.16	–6.64	122.3	1.18	0.132	–27.1
	56	278.83908	2.18	17.58	–48.86	93.4	1.88	0.167	nd
	60	279.00269	1.98	14.12	43.05	81.2	1.26	0.100	–26.9
		Average	*1.95*	*15.82*	*10.07*	*96.0*	*1.34*	*0.13*	*–27.9*
		Std. Error	*0.08*	*1.37*	*19.65*	*5.7*	*0.11*	*0.01*	*0.39*
WB6 mid	30	277.93727				nd	nd	nd	nd
	35	278.09740	5.41	10.95	65.34	151.3	1.92	0.180	–28.5
	39	278.24064	3.86	21.47	–50.03	143.9	3.96	0.316	–27.3
	44	278.39914	4.79	17.60	–8.91	101.9	1.77	0.169	–28.5
	48	278.53879	4.31	19.59	99.05	120.7	1.95	0.169	–28.1
	52	278.69892	3.38	22.08	–1.57	132.3	1.28	0.130	–26.9
	56	278.83908	4.55	20.34	–41.28	182.2	2.09	0.165	–28.0
	60	279.00269	6.17	18.45	78.69	107.4	1.21	0.088	–27.2
		Average	*4.64*	*18.64*	*20.18*	*134.2*	*2.02*	*0.17*	*–27.8*
		Std. Error	*0.35*	*1.41*	*22.74*	*10.5*	*0.35*	*0.03*	*0.24*
WB6 deep	30	277.93727	7.88	10.90	33.10	94.1	1.39	0.122	–28.5
	35	278.09740	9.07	10.88	55.88	148.5	2.27	0.135	–27.0
	39	278.24064	8.17	22.56	–20.62	108.9	1.06	0.100	–29.2
	44	278.39914	8.28	21.06	4.08	112.6	1.64	0.169	–30.7
	48	278.53879	8.53	20.57	62.63	162.3	2.69	0.262	–26.9
	52	278.69892	8.83	25.52	26.89	239.9	3.41	0.204	–28.1
	56	278.83908	8.49	25.46	–2.19	147.9	1.70	0.113	–27.3
	60	279.00269	9.15	24.79	45.18	210.0	3.96	0.279	–25.1
		Average	*8.55*	*20.22*	*25.62*	*153.0*	*2.27*	*0.17*	*–27.4*
		Std. Error	*0.16*	*2.14*	*10.44*	*17.9*	*0.361*	*0.024*	*0.6*

Table 1 (*continued*)

	Cast	Jul Date	Depth (m)	Salinity (psu)	Current (cm sec^{-1})	TSS (mg L^{-1})	POC (mg L^{-1})	PN (mg L^{-1})	$\delta^{13}C$ (per mil)
WB7 surface	36	278.12996	2.46	15.42	54.74	97.1	1.23	0.148	–30.9
	40	278.28173	2.59	14.27	–90.38	53.1	0.91	0.085	–29.4
	45	278.43109	2.08	14.40	–46.63	57.1	1.02	0.100	–30.4
	49	278.57352	2.66	14.54	78.76	97.8	1.82	0.174	–28.3
	53	278.72919	1.83	13.73	–1.18	118.8	1.20	0.108	–27.8
	57	278.88138	5.12	13.40	–82.51	91.6	2.10	0.193	–28.2
	61	279.03233	2.05	12.82	53.70	76.0	1.50	0.140	nd
	65	279.15448	2.49	16.082	50.09	101.9	1.66	0.112	–27.4
		Average	*2.66*	*14.33*	*2.07*	*86.7*	*1.43*	*0.13*	*–28.7*
		Std. Error	*0.37*	*0.37*	*23.80*	*8.1*	*0.15*	*0.01*	*0.50*
WB7 mid	36	278.12996	5.38	15.69	41.66	133.0	1.84	0.168	–27.7
	40	278.28173	4.12	14.78	–81.68	54.3	0.97	0.091	–28.9
	45	278.43109	5.37	14.59	–22.74	76.6	1.37	0.137	–27.9
	49	278.57352	4.95	16.85	67.75	197.8	2.88	0.257	–26.4
	53	278.72919	3.97	13.72	–14.12	152.3	1.19	0.105	–27.8
	57	278.88138	6.40	15.32	–80.96	107.7	2.26	0.177	–27.2
	61	279.03233	4.88	15.43	74.28	109.9	2.00	0.190	–27.2
	65	279.15448	7.260	17.195	38.160	149.4	0.79	nd	–26.8
		Average	*5.29*	*15.45*	*2.79*	*122.6*	*1.66*	*0.16*	*–27.3*
		Std. Error	*0.39*	*0.41*	*22.03*	*16.1*	*0.25*	*0.02*	*0.27*
WB7 deep	36	278.12996	8.91	15.80	32.58	404.5	4.97	0.435	–26.7
	40	278.28173	5.84	17.45	–83.13	65.7	1.21	0.110	–28.7
	45	278.43109	8.12	14.58	1.96	91.0	2.11	0.200	–29.2
	49	278.57352	8.58	17.57	47.66	256.3	7.34	0.490	–27.2
	53	278.72919	7.82	14.27	–16.17	168.3	1.34	0.114	–29.3
	57	278.88138	7.43	15.62	–64.00	173.8	3.63	0.274	–26.2
	61	279.03233	8.11	18.02	43.89	151.8	4.66	0.363	–26.8
	65	279.1544809	9.44	16.533	37.25	249.2	9.30	0.579	–28.6
		Average	*8.03*	*16.23*	*0.01*	*195.1*	*4.32*	*0.32*	*–27.6*
		Std. Error	*0.38*	*0.49*	*17.89*	*38.1*	*1.02*	*0.06*	*0.44*
WB8 surface	33	277.99855	3.84	10.42	47.67	83.4	1.33	0.169	–29.5
	37	278.15620	2.73	15.78	38.68	92.4	1.16	0.108	–30.1
	42	278.31655	3.22	12.39	–58.01	70.9	1.87	0.177	–28.9
	46	278.45386	1.91	8.26	–10.18	46.5	1.13	0.107	–30.0
	50	278.59966	1.95	12.66	70.34	77.2	1.61	0.160	–29.0
	54	278.75495	2.55	16.89	–45.91	106.4	1.38	0.113	–28.2
	58	278.91709	0.84	9.37	–55.64	57.2	1.23	0.087	–28.9
	62	279.05266	6.42	16.02	69.87	142.8	4.56	0.349	–26.1
		Average	*2.93*	*12.72*	*7.10*	*84.6*	*1.78*	*0.16*	*–28.2*
		Std. Error	*0.59*	*1.15*	*19.76*	*10.7*	*0.41*	*0.03*	*0.44*
WB8 mid	33	277.99855	7.73	10.53	44.49	88.5	2.69	0.250	–27.9
	37	278.15620	7.37	17.95	31.71	152.8	1.42	0.146	–30.3
	42	278.31655	4.86	12.82	–50.80	79.3	2.26	0.207	–28.8
	46	278.45386	5.40	12.34	12.99	nd	1.40	0.157	–28.4
	50	278.59966	4.07	14.21	90.51	121.8	1.35	0.197	–27.5
	54	278.75495	5.34	18.69	–40.40	109.3	1.52	0.112	–29.5
	58	278.91709	3.99	10.98	–34.50	73.8	1.72	0.153	–28.9
	62	279.05266	8.24	16.52	45.74	230.3	6.22	0.390	–26.3
		Average	*5.88*	*14.26*	*12.47*	*122.3*	*2.32*	*0.20*	*–27.9*
		Std. Error	*0.59*	*1.11*	*17.73*	*20.8*	*0.58*	*0.03*	*0.44*
WB8 deep	33	277.99855	8.62	10.54	37.65	100.6	4.82	0.418	–28.1
	37	278.15620	9.05	18.05	25.36	nd	2.77	0.247	–27.9
	42	278.31655	6.56	13.24	–47.81	78.1	2.25	0.200	–28.8
	46	278.45386	8.02	13.11	11.36	90.7	1.89	0.200	–28.3
	50	278.59966	7.97	16.64	58.80	173.1	3.87	0.230	–26.5
	54	278.75495	7.39	19.16	–37.51	114.3	1.82	0.132	–26.2
	58	278.91709	7.96	13.08	–21.04	155.6	4.36	0.291	–26.6
	62	279.05266	9.63	17.05	38.76	281.1	9.36	0.641	–27.3
		Average	*8.15*	*15.11*	*8.20*	*141.9*	*3.89*	*0.295*	*–27.4*
		Std. Error	*0.34*	*1.07*	*13.85*	*26.6*	*0.879*	*0.058*	*0.3*

Captions: Julian Dates and water depth are indicated for each hydrocast; along channel current measured at each sampling depth; TSS, total suspended sediment concentration; POC, particulate organic carbon concentration; PN, particulate nitrogen concentration; $\delta^{13}C$, stable carbon isotope composition of POC; nd, no data. Average and standard error (Std. Error = average/$n^{1/2}$) are given for each sample series. *Tidally averaged $\delta^{13}C$ calculated according to Eq. (3) in the text.

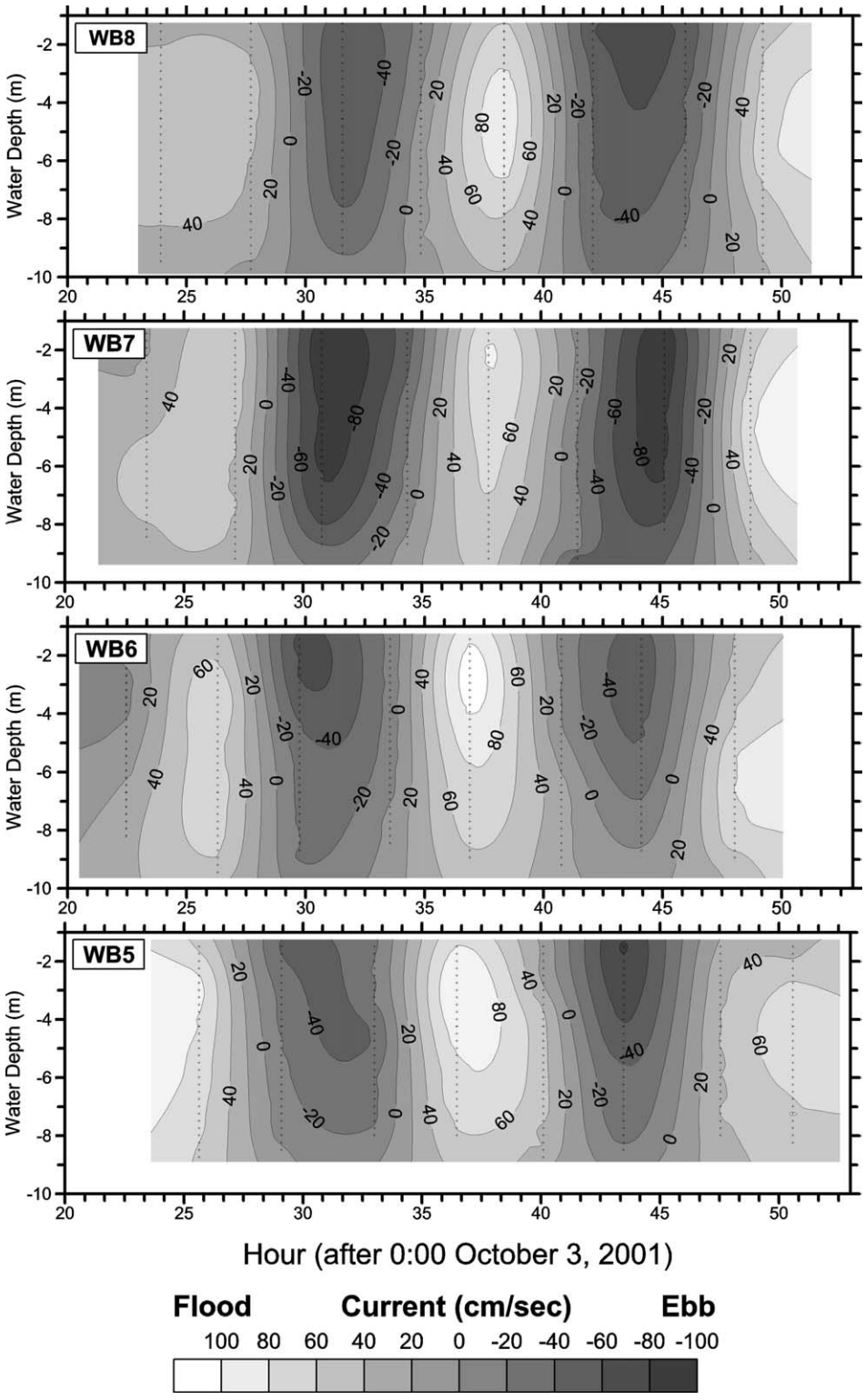

Fig. 2. Along-channel current velocity profiles for each station over two tidal cycles. Vertical lines within each figure represent the time of each cast. Landward flow (up the estuary) is indicated by positive along-channel velocities whereas seaward flow (down the estuary) is indicated by negative along-channel velocities.

WB7 (87 to 195 mg L^{-1}). Other stations, such as WB6 and WB8 also exhibited significant increases in TSS* with depth (96–153 and 85–142 mg L^{-1}, respectively). The differences with depth in TSS* concentrations were least prominent (but still statistically significant, $p < 0.10$) at the seaward-most station, WB5, where tidally averaged values for the surface and deep were 130 mg L^{-1} and 170 mg L^{-1}, respectively (Fig. 5a).

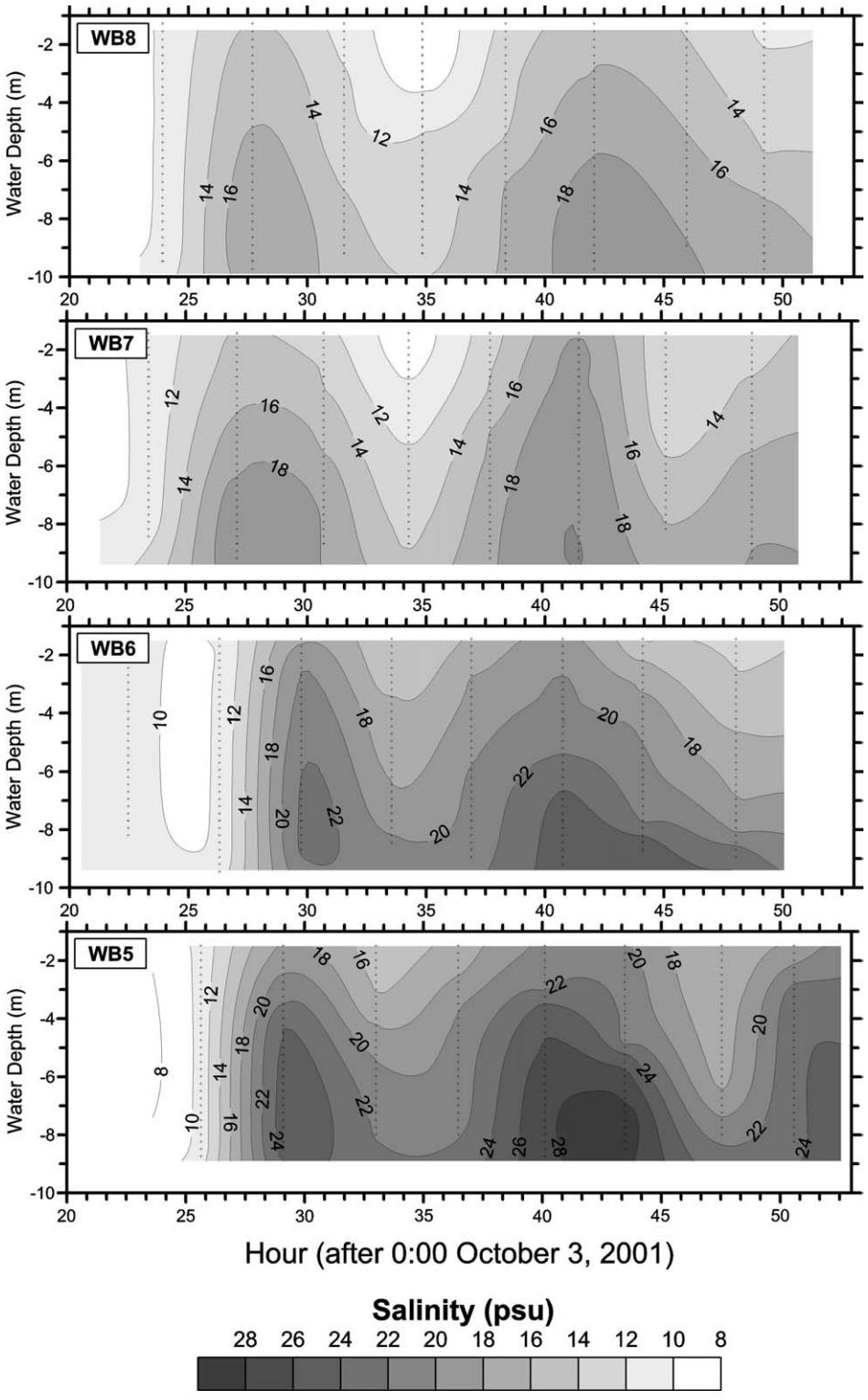

Fig. 3. Salinity profiles for each station over one tidal cycle. Vertical lines within each figure represent the time of each cast.

3.2.2. Particulate organic carbon concentrations

POC concentrations also varied over one order of magnitude among stations during the study period, ranging from 0.8 mg L^{-1} at WB7 mid to 9.3 mg L^{-1} at WB7 and WB8 deep (Table 1). Similarly to the patterns in surface TSS, there was little variability in POC concentrations of the surface samples with magnitude or direction of the tide (plots not shown). For example, at

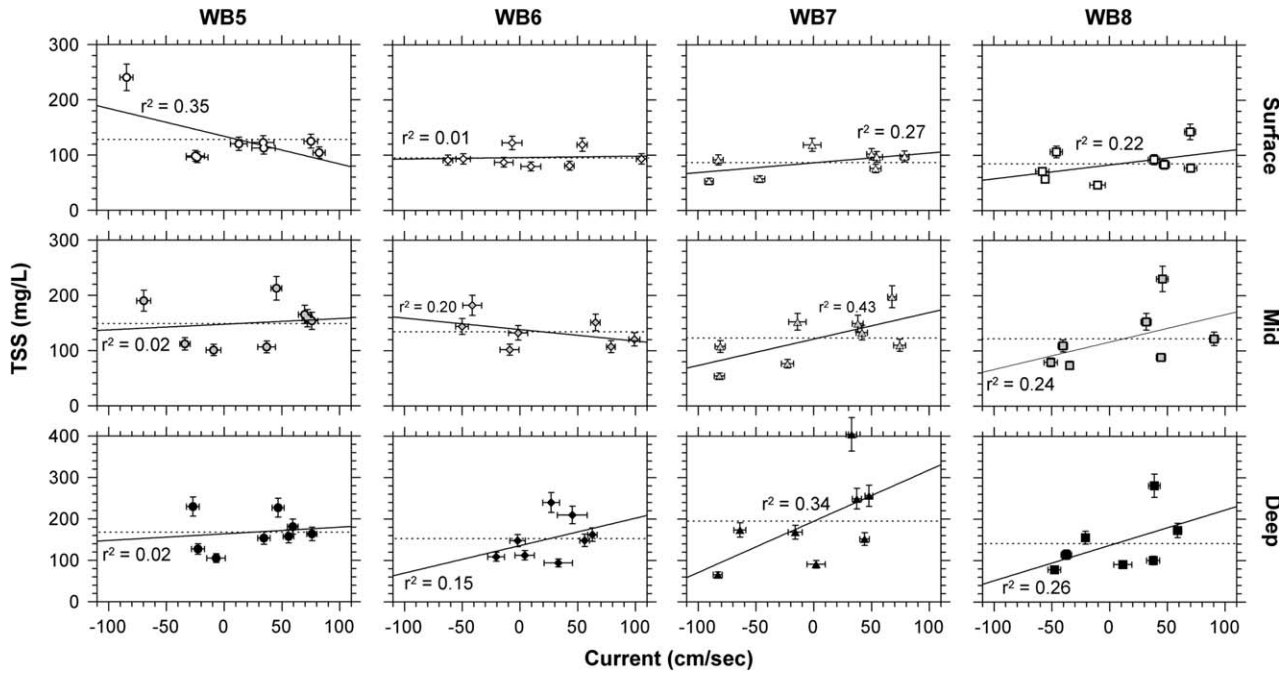

Fig. 4. Distribution of total suspended sediment (TSS) concentrations (mg L^{-1}) as a function of current speed and direction for the three water column depths of the four Winyah Bay stations. All data are from Table 1. The linear correlation coefficients between TSS and current at each station are plotted next to the correlation line. Error bars represent the standard deviation of each measurement.

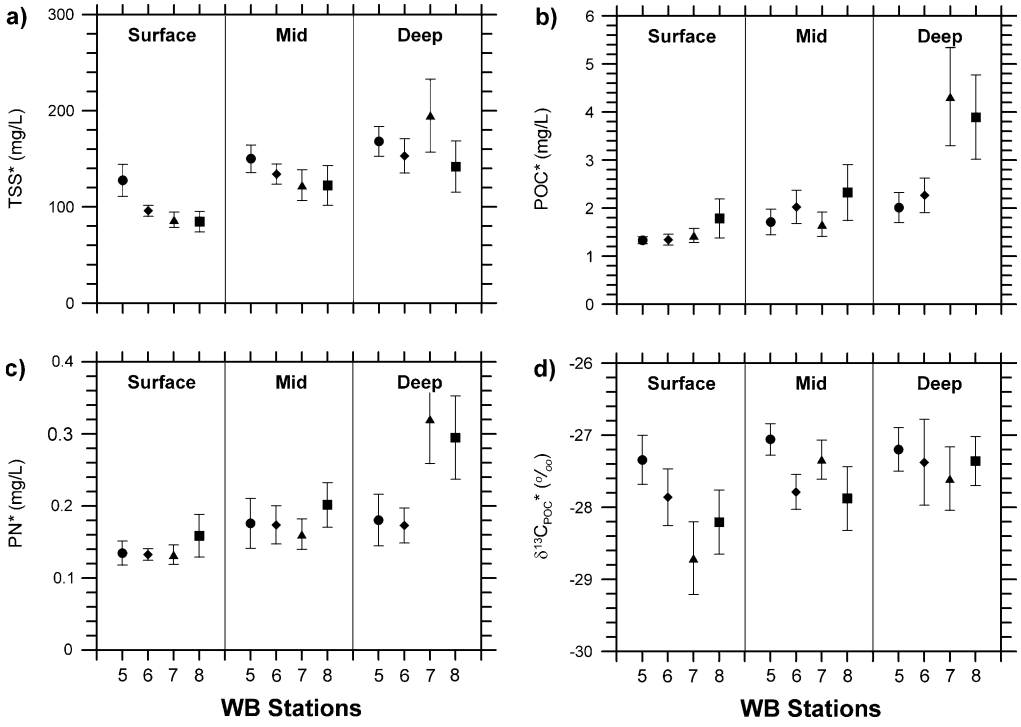

Fig. 5. Tidally averaged values of (a) total suspended sediment (TSS*) concentration, (b) particulate organic carbon (POC*) concentration, (c) particulate organic nitrogen (PON*) concentration, and (d) stable carbon isotopic composition of POC ($\delta^{13}C_{POC}$*) for surface, mid and deep samples at the four Winyah Bay stations. Error bars represent variability (standard error) over the two tidal cycles.

WB5, while surface current velocities ranged from −80 to 80 cm s^{-1}, POC concentrations only ranged from 0.9 to 1.7 mg L^{-1}. In contrast, the strongest correlations between POC concentration and current direction and magnitude were observed for the deep samples, particularly at WB6, WB7 and WB8 where POC concentrations were positively correlated with flood currents (r^2 of 0.37, 0.48 and 0.25, respectively). POC concentrations in most stations were generally higher ($p < 0.10$) during flood tide than during the ebb. As with TSS, POC was poorly correlated with salinity indicating non-conservative mixing.

In contrast to TSS*, tidally averaged POC (POC*) concentrations did not decrease up the estuary but rather showed slight increases (Fig. 5b). For example, surface POC* concentrations in WB8 (1.8 mg L^{-1}) were higher than in WB5 (1.3 mg L^{-1}). In the case of the deep samples, POC* concentrations in WB8 were also higher than in WB5 and WB6 (3.9 vs. 2.0 and 2.3 mg L^{-1}, respectively) although the difference was less statistically robust ($p < 0.10$). As was the case for TSS*, there were marked contrasts in POC* concentrations with depth at each station, with the deep samples always displaying the highest concentrations (Fig. 5b). Similarly to TSS, the largest contrasts in POC* concentrations were measured between surface and deep samples at WB7 and WB8, which displayed statistically significant differences between surface and deep samples (1.4 vs. 4.3 and 1.8 vs. 3.9 mg L^{-1}, respectively). The contrasts in POC* surface and deep samples were also significantly different at WB6 ($p < 0.05$) and WB5 ($p < 0.10$).

3.2.3. Particulate nitrogen concentrations

PN concentrations for all samples ranged from 0.08 mg L^{-1} at WB5 surface to 0.62 mg L^{-1} at WB8 deep. As was the case for POC, surface PN concentrations at all four stations did not show significant trends with current magnitude and direction (plots not shown). Like POC, the most significant trends between PN concentrations and current were observed in the deep stations, where positive linear correlations between these parameters displayed elevated r^2 coefficients of 0.3–0.6. Elevated correlation coefficients between PN and currents ($r^2 > 0.4$) were also observed at WB6 mid. Overall, PN concentrations measured during flood tide were significantly higher ($p < 0.1$) than during the ebb tide.

The spatial variability in tidally averaged PN (PN*) concentrations was relatively small (Fig. 5c), with values ranging from 0.13 mg L^{-1} at WB5 surface to 0.32 mg L^{-1} at WB7 deep. All stations displayed comparable PN* concentrations in surface and mid samples, with only the deep samples exhibiting statistically significant differences ($p < 0.1$) between the lower bay stations (WB5 and WB6) and the upper bay stations (WB7 and WB8) (Fig. 5c). As was the case for TSS* and POC*, PN* concentrations also exhibited slight increases with depth at every station, although because of the relatively high variability these differences were only significant ($p < 0.1$) for the WB7 and WB8 stations.

3.2.4. Particulate organic carbon isotopic compositions

$\delta^{13}C_{POC}$ values ranged from −25‰ at WB6 deep to −31‰ at WB7 surface (Table 1). In general, there were no consistent statistical relationship between $\delta^{13}C_{POC}$ values and current, although in a few stations we observed slight enrichments in the isotopic composition of POC in samples collected during maximum flood. For example, WB5 mid, WB6 deep, WB7 mid and WB8 mid all displayed positive linear correlations (plots not shown) between $\delta^{13}C_{POC}$ values and current with elevated correlation r^2 coefficients (0.6, 0.4, 0.4 and 0.3, respectively). The magnitude of isotopic enrichment from maximum ebb to maximum flood ranged from 1 to 4‰ (Table 1). Similarly to other parameters, there was no significant relationship between salinity and $\delta^{13}C_{POC}$ values. The only exceptions were the trends of slight enrichment in $\delta^{13}C_{POC}$ with increased salinity (r^2 of 0.5) exhibited by the samples at WB6 mid and W7 mid.

In order to estimate the tidally averaged isotopic signatures at each station, we used an isotopic mass balance approach to weigh the $\delta^{13}C_{POC}$ composition of each sample by its POC concentration according to the following equation:

$$\delta^{13}C^{*}_{POC}(z) = \sum_{i=1}^{n} (\delta^{13}C_s(z,t_i) f_{POC}(z,t_i)) \quad (3)$$

where $\delta^{13}C^{*}_{POC}$ is the tidally-integrated stable carbon isotopic composition at each sampling depth z. $\delta^{13}C_s$ is the stable carbon isotopic value for each sample and f_{POC} is the fraction of the total particulate organic carbon inventory at each station and depth and time t_i. The subscript i denotes the discrete sample collected at time t_i at the elevation z and particular station. f_{POC} was calculated using:

$$f_{POC}(z,t_i) = c(z,t_i) \Big/ \sum_{i=1}^{i=n} c(z,t_i) \quad (4)$$

where c is the POC concentration.

The $\delta^{13}C^{*}_{POC}$ signatures of samples collected from all stations ranged from −29‰ to −27‰ (Fig. 5d). Spatially, we observed significant landward depletions in the $\delta^{13}C^{*}_{POC}$ signatures of surface and mid samples up the estuary, from values of about −27‰ at WB5 to values less than −28‰ at WB8. A similar trend was not observed in the deep samples, all of which displayed comparable $\delta^{13}C^{*}_{POC}$ signatures of ca. −27.5‰ (Fig. 5d). In terms of contrasts with depth, the lower estuary stations (WB5 and WB6) displayed similar $\delta^{13}C^{*}_{POC}$ values for surface, mid and deep samples

(Fig. 5d). On the other hand, there were differences in the $\delta^{13}C^*_{POC}$ signatures of the surface, mid and deep samples from the upper estuary stations, with the deep values being significantly enriched in ^{13}C at both WB7 ($p < 0.1$) and WB8 ($p < 0.05$) relative to their surface counterparts.

4. Discussion

4.1. Tidally-integrated local fluxes

In order to understand the fate of suspended sediments and particulate organic matter in the vicinity of the turbidity maximum, measurements of current velocity and the chemical measurements of concentration were combined to calculate instantaneous local fluxes (F) at the three sampling depths in each station using the following equation:

$$F(z,t_i) = c(z,t_i) \cdot U(z,t_i) \quad (5)$$

where, c represents salt, TSS, POC or PN concentration and U is the along-channel current velocity, t_i is the time of sampling and z indicates the depth of sampling. Current velocity values at each depth were extracted from the ADCP profiles (see Table 1).

Based on these results, tidally-integrated fluxes at each depth, $F^*(z)$ were calculated for each station for a period of two tidal cycles (24.8 h) using:

$$F^*(z) = \left[\frac{\sum_{i=1}^{i=n} (F(z,t_i)\Delta t_i)}{\sum_{i=1}^{i=n} \Delta t_i} \right] \quad (6)$$

where $F(z,t_i)$ is the instantaneous flux at each measurement i (see Eq. (5)). Δt_i is the time period represented by each observation calculated as:

$$\Delta t_i = \left(\frac{(t_i - t_{i-1}) + (t_{i+1} - t_i)}{2} \right) \quad (7)$$

Before examining the net fluxes of particulate materials, it is important to discuss the net transport of salt in the context of this study. Tidally-integrated fluxes of salt show a net landward flux (positive fluxes indicate transport up the estuary) in the deeper parts of the water column (mid and deep samples) at WB5 and WB6 (Fig. 6a). In contrast, net salt fluxes are close to zero throughout the water column at WB7 and WB8, indicating that this part of the estuary is in near steady state in terms of salt transport. The apparent net importation of salt through the deeper part of the channel in the lower region of the estuary may be due to our sampling being restricted to the central navigation channel of the bay. Studies of the overall circulation in this region of Winyah Bay during low river discharge conditions (Kim and Voulgaris, submitted for publication) indicate that a significant portion of water and salt transported landward during the flood tide is discharged seaward along the western channel in this part of the estuary (Fig. 1). Thus, the estimated local landward salt fluxes at WB5 and WB6 are controlled by the asymmetry of ebb and flood velocities and the residual flows that develop in the main channel as result of the estuarine and channel morphology (Kim and Voulgaris, submitted for publication).

The observed net salt fluxes provide us with a reference for conservative material flux from which to evaluate the transport of potentially non-conservative components such as TSS, POC and PN (Fig. 6b–d). Overall, these calculations show net tidally integrated landward fluxes of TSS, POC and PN in the deeper portions of the water column at all four stations along the main channel of the bay. As was the case for salt, the net fluxes of particulate materials in the surface of most stations are statistically undistinguishable from zero (Fig. 6). In all the stations, the highest TSS*, POC* and PN* fluxes occur in deep portions of the water column, where they range from 100 to 350 g cm^{-2} d^{-1}, from 4 to 6 g cm^{-2} d^{-1} and from 0.3 to 0.6 g cm^{-2} d^{-1}, respectively. Most significantly, while the patterns of TSS*, POC* and PN* fluxes are similar to those of net salt fluxes in the lower part of the estuary (WB5 and WB6), there are marked differences in the upper bay stations (WB7 and WB8), which are closer to the ETM. For example, in these locations, TSS* and especially POC* and PN* fluxes are significantly higher than zero whereas net salt fluxes are close to zero (Fig. 6). Such contrasts are evidence for the non-conservative nature of particulate transport in the upper region of Winyah Bay, where the ETM was located at the time of the study.

It is important to note that all flow measurements presented in this manuscript are Eulerian in nature and represent conditions at the sampling point only (i.e., local fluxes). In case of a progressive wave, Lagrangian velocities can be estimated theoretically using point measurements (Longuet-Higgins, 1989). However, this is not possible in an estuarine environment where the tidal wave is influenced by complex bathymetry and channel length (Zimmerman, 1979; Cheng and Casulli, 1982; Jay, 1991). Thus, geochemical transformations occurring during the transport of material (Lagrangian transformations) cannot be resolved directly and it is not possible to quantitatively interpret the differences in net local fluxes along the estuary. However, insights on the processes controlling the particulate fluxes are evident if we consider the differential behavior of TSS and POC (and PN) in the region close to the ETM. For example, the TSS* fluxes in the deeper portions of the water column are significantly attenuated in WB7 and WB8 relative to the POC* and PN* fluxes (Fig. 6).

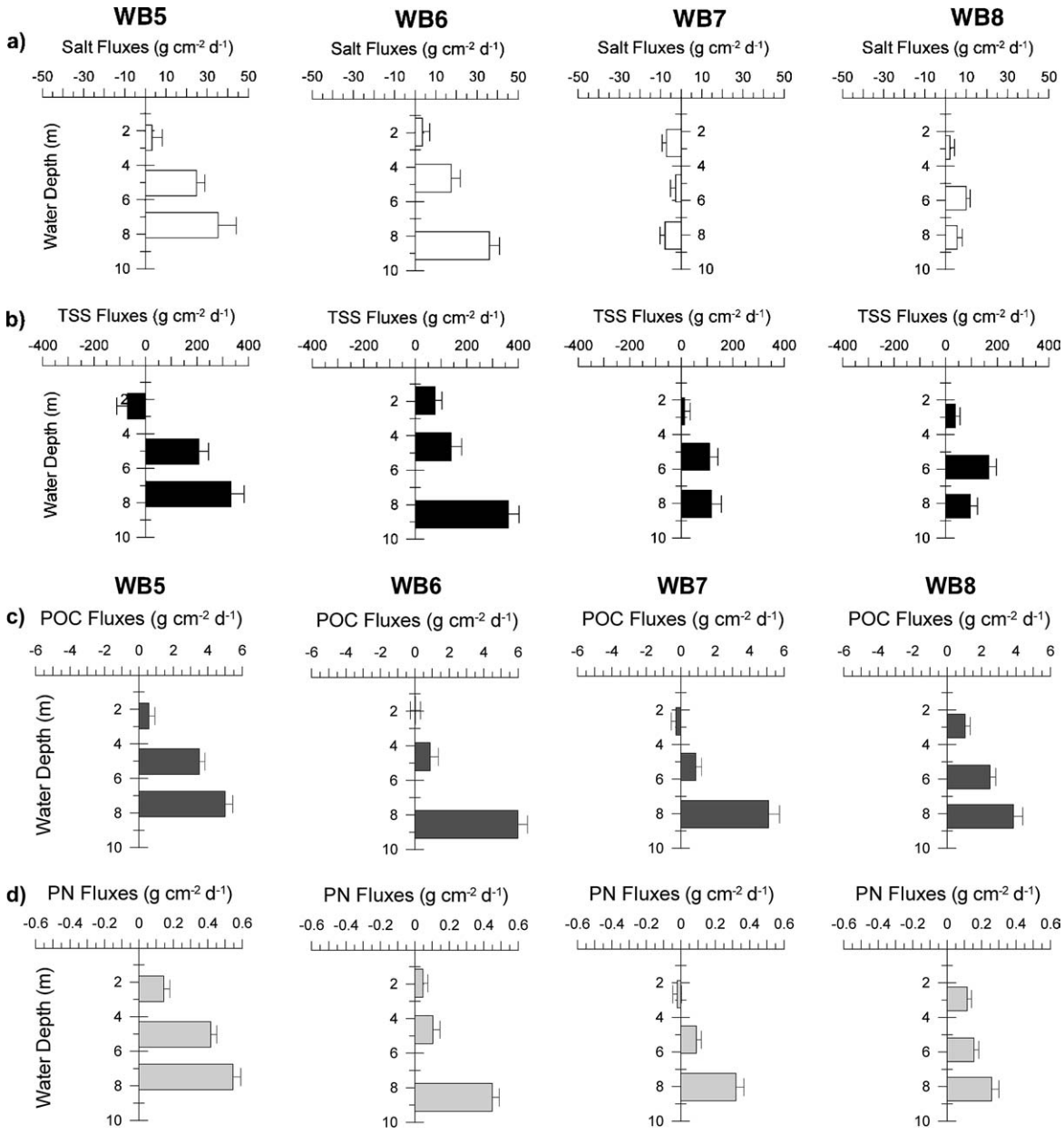

Fig. 6. Plots of tidally-integrated fluxes of (a) salt, (b) TSS, (c) POC, and (d) PN. The bars represent surface, mid, and deep portions of the water column. Positive fluxes indicate a net landward transport up the estuary and negative fluxes indicate a net seaward transport of material. The error bars represent the standard error of the integrated fluxes.

Hence, it appears that POM is transported more efficiently relative to TSS up the estuary in the region around the ETM (WB7 and WB8), suggesting inorganic sediment is being trapped in this part of Winyah Bay.

The apparent differential transport of mineral and organic particles in the vicinity of the ETM has significant biogeochemical consequences. For example, in this part of the estuary, particles are periodically exposed to oxygenated water, which facilitates the oxidation of metal-oxide phases and can lead to enhanced POM degradation (Aller, 1994, 1998). Therefore, under the conditions of low river discharge encountered in Winyah Bay during this study period, we could expect enhanced rates of POM mineralization and solubization (Komada and Reimers, 2001) as materials are transported up the estuary by the flood-dominated sediment transport regime. On the other hand, the preferential transport of POC and PN relative to TSS observed near the ETM suggest that particle trapping preferentially sequesters higher density particles with lower OM contents in the seabed, allowing OM-rich, finer material of lower density to be carried further up the estuary. It is also possible that sorption of DOM onto particles during the flooding stages of the

tide, when turbidity is highest, may also transfer additional DOM to the particles thus resulting in a net landward flux of POM. Deciphering among these possibilities requires a better understanding of temporal and spatial variability of POM composition in this region of Winyah Bay.

4.2. Nature of suspended particles

To gain information on how the organic carbon loading of suspended particles changes tidally along the estuary, we calculated the weight percent organic carbon content of suspended particles (%POC = (POC/TSS) × 100). The data from Table 1 indicate that %POC values ranged from 0.5% at WB5 mid to 4.8% at WB8 deep. Although there were no clear statistical trends between %POC and current when all the data set is considered, the samples from WB6 deep exhibited a significant correlation between current and %POC ($r^2 = 0.7$, plot not shown), with the highest %POC values measured during high flood velocities.

To assess the overall effect of the landward flux on the OM loadings of particles, we calculated the tidally averaged %POC (%POC*) content of suspended particles at different depths and locations of Winyah Bay (Fig. 7a). These calculations clearly show that %POC* contents increase significantly up the estuary at all depths. For example, in surface waters, %POC* contents increase from ~1% (WB5) to about ~2% (WB8). Similar trends are evident for samples from the mid-water column. In the case of the deep samples, %POC* values increase from ~1% in WB5 to almost 3% in WB8. Notably, unlike the TSS* and POC* concentrations (Fig. 5), there are no statistically significant differences in the %POC* values of particles from different depths within each station (Fig. 7a).

These observations indicate that the net landward transport of particles up Winyah Bay results in the sorting of particles with different organic matter loadings. It is likely that the higher %POC contents in the upper reaches of the estuary reflect the resuspension and preferential transport of organic matter-rich particles of lower density under the flood-dominant regime that characterized this period. We suggest that higher density particles with lower %POC are transported less efficiently and, therefore, are more abundant in the lower reaches of the study area under the flow conditions at the time of sampling. Such results do not support a decrease in the %POC content of particles due to microbial and leaching losses during their resuspension and transport up the estuary. It is possible that carbon losses from particles through degradation and solubilization still occur. However, the hydrodynamic sorting of particles with different carbon loadings hinders our ability to detect such changes in the bulk particle pool.

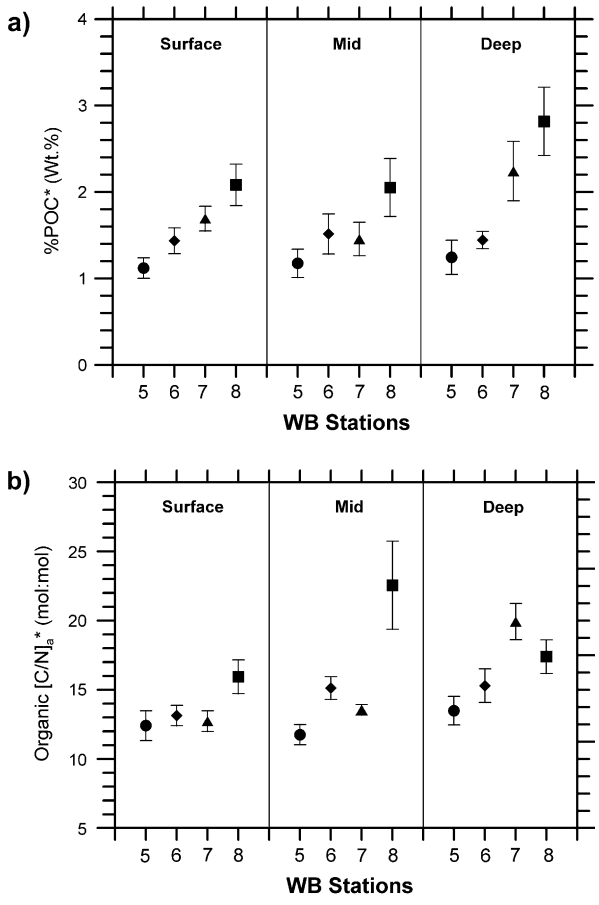

Fig. 7. Tidally averaged values of (a) % organic carbon content of suspended particles (%POC*) and (b) atomic organic carbon:nitrogen ratios (org[C:N]$_a$*) for surface, mid and deep samples at the four Winyah Bay stations. Error bars represent the standard error over the two tidal cycles.

4.3. Sources of particulate organic matter

Elemental atomic ratios of organic carbon and nitrogen ([C/N]$_a$) are often used to gain a better understanding of the origin of organic matter. Before applying the [C/N]$_a$ to elucidate POM sources, it is important to account for the presence of inorganic nitrogen (Hedges et al., 1986; Goñi et al., 1998, 2003). In Fig. 8, PN concentrations are plotted against POC concentrations at each sampling location. Samples from the lower bay (WB5) display a positive POC intercept at zero PN, indicating that all the nitrogen present in the samples appears to be associated with organic matter. In contrast, plots for WB6 mid, WB7 deep and all depths at WB8 reveal a positive nitrogen intercept at zero POC. The magnitude of this intercept is an indication of the amount of particulate inorganic nitrogen (PIN) in the samples (Hedges et al., 1986; Ruttenberg and Goni, 1997; Goñi et al, 1998, 2003). It is likely that PIN includes ammonium adsorbed on to inorganic mineral surfaces such as negatively charged fine clays (Müller, 1977), which under the flow conditions encountered at

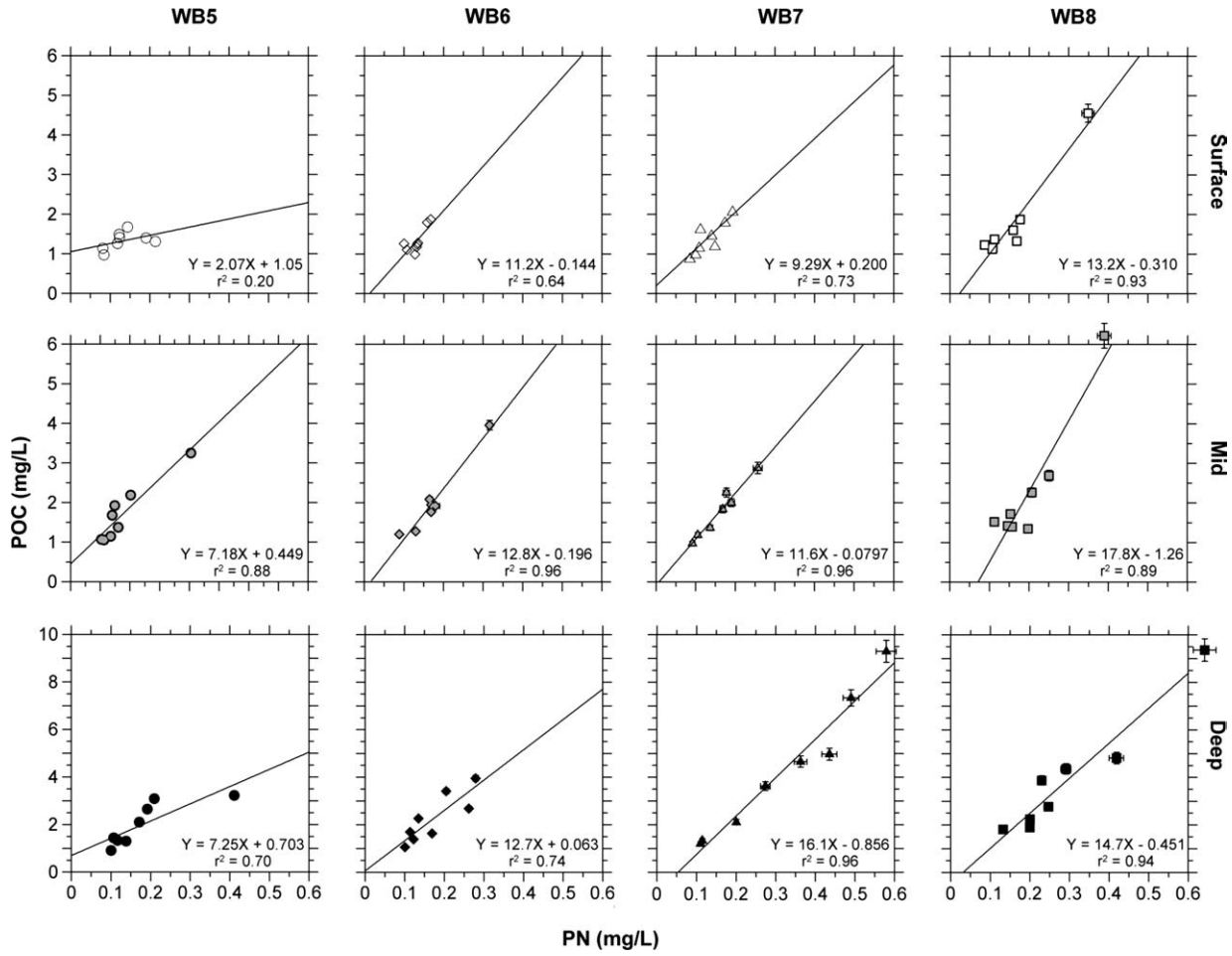

Fig. 8. Plots of POC vs. PN for all sampling depths and locations. The linear fit between the two variables is included in each graph. The positive intercept at zero organic carbon indicates presence of nitrogen that is not associated with organic matter. When error bars are missing it is because they are smaller than the size of individual data point symbols.

the time of sampling may be preferentially transported up the estuary due to their lesser density. Furthermore, if this PIN pool represents ammonium derived from the mineralization of organic nitrogen, the increase measured up estuary may be consistent with enhanced OM mineralization during particle resuspension and transport (e.g., Aller, 1998).

Organic PN concentrations, which were calculated for each sample as the difference between PN and PIN (Hedges et al., 1986; Goñi et al., 1998, 2003), were used to estimate the atomic carbon:nitrogen ratios of the organic matter in all samples. Organic $[C/N]_a$ ratios ranged from 7 at WB5 surface to 27 at WB7 deep. For the most part, there was no obvious correlation between organic $[C/N]_a$ ratios and currents, although the samples from WB7 deep and WB8 surface and mid displayed slight decreases in C/N ratios with current magnitude (r^2 of 0.3; plots not shown).

Tidally averaged organic $[C/N]_a$ ratios (org$[C/N]_a$*) ranged from 12 at WB5 mid to 23 at WB8 mid (Fig. 7 b). There were significant increases in org$[C/N]_a$* from the lower (WB5) to the upper part (WB8) of the Winyah Bay at all three depths. These data indicate that the hydrodynamic sorting mechanism responsible for the net landward transport of particles with greater organic matter loadings up the estuary (Fig. 7 a) appears to be preferentially moving particles with higher organic C/N ratios. Since organic matter enriched in vascular plant detritus is typically characterized by elevated org[C:N]a ratios, these results are consistent with the preferential mobilization of organic-rich particles with significant vascular plant detritus contents. The high org$[C/N]_a$* ratios (>20) displayed by the mid and deep samples from WB7 and WB8 (Fig. 7b), indicates that this transport predominantly occurs near the bed.

It is possible to use the elemental ratios of the organic matter in combination with the isotopic composition of the organic carbon (Keil et al., 1994; Goñi et al., 2003) to further discriminate the sources of the organic materials in the water column of Winyah Bay. Fig. 9

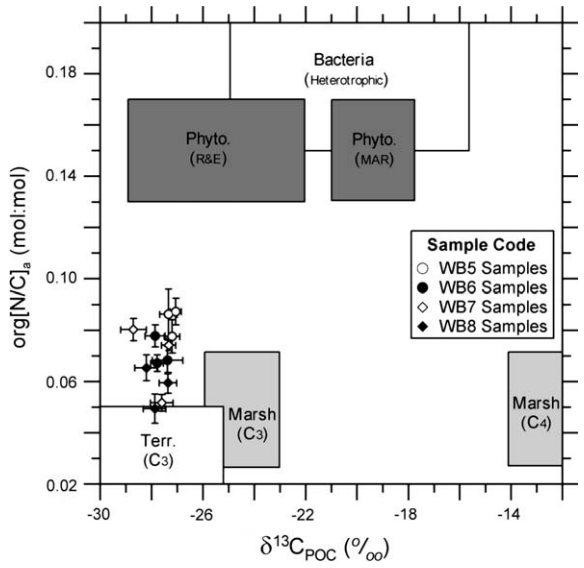

Fig. 9. Plot of atomic organic nitrogen:carbon ratios (org[N:C]$_a$) versus the stable carbon isotopic compositions ($\delta^{13}C_{POC}$) of suspended particles. Data points are tidally averaged values for each station at each depth. Error bars represent the standard error over the two tidal cycles. Also plotted are the compositional ranges of potential end member sources for Winyah Bay (after Goñi et al., 2003).

shows a plot of the tidally averaged atomic N/C ratios of organic matter (org[N/C]$_a$*) vs. $\delta^{13}C^*_{POC}$ compositions for all depths at the four stations in the estuary. Also plotted are the compositional ranges for locally important organic matter sources (Teixeira, 2000; Goñi et al., 2003 and references therein). In this graph, we plot org[N/C]$_a$* rather than its reciprocal because this ratio is statistically more robust since the larger number (POC) is in the denominator. Additionally, it allows us to plot two parameters that are essentially carbon normalized (N/C and $^{13}C/^{12}C$ ratios). All of the samples in Fig. 9 plot between the C_3 terrestrial plants and riverine/estuarine phytoplankton end member regions, indicating that there is little or no contribution from C_4 marsh grasses and marine phytoplankton.

Although one has to be careful when interpreting these data because diagenetic reactions can change both the elemental and isotopic ratios of the original organic matter, it appears that during the study period most of the POM in this part of Winyah Bay originated from river/terrigenous sources. Using a simple two-end member mixing model (e.g. Goñi et al., 2003), it is possible to draw qualitative estimates of the relative contributions from terrigenous vascular C3 plant sources ([N/C]$_a$ = 0.0275) and from riverine/estuarine phytoplankton end members ([N/C]$_a$ = 0.146). These estimates suggest that organic matter from terrigenous C_3 plant sources contribute 50–65% of the POM in the lower estuary stations (WB5 and WB6) and 60–80% of the POM in the upper estuary station (WB7 and WB8). As expected from the previous discussion, the highest terrigenous contributions are in the deeper portions of the water column at WB7 and WB8. The reduced riverine/estuarine phytoplankton POM contributions calculated for samples from the upper reaches of Winyah Bay may reflect the higher lability and preferential degradation of this material as particles are transported landward up the estuary.

How do we explain the net landward transport of terrigenous POM along the main channel of Winyah Bay at the time of our study? We speculate that this POM was probably delivered to the lower reaches of the estuary during past periods of higher discharge. A moderate peak in discharge that occurred days prior to the cruise and the seasonal peak of high discharge during March–April may be likely candidates. Additionally, as previously mentioned, the circulation in the central part of the Winyah Bay may provide an additional mechanism for the input of river-derived particles to locations south of WB5 (Fig. 1). Kim and Voulgaris (submitted for publication) found that in this region of Winyah Bay a significant fraction of the water flux during ebb is through a narrow channel located to the west of the island to the south of WB5 (Fig. 1). In contrast, the central navigation channel acts as a conduit for landward delivery of seawater and suspended materials during the flooding tide. This mechanism creates a circular residual current around this small island and may represent a conduit for river-borne particles to reach the central part of Winyah Bay.

The net landward flux of sediments and POM during low discharge, which may be enhanced by the residual circulation under these low flow conditions, represents an efficient mechanism of particle trapping that likely enhances the mineralization of river- and land-derived organic matter prior to its burial in estuaries or export to the ocean. In contrast, we anticipate that during periods of high river discharge the net transport of sediments and POM will be in the seaward direction, leading to the export of river-derived materials to the lower reaches of Winyah Bay and the coastal ocean. Our results reinforce the importance of physical forcing mechanisms (river discharge, tidal amplitude, wind) in determining the balance between landward and seaward transport of particulate materials in this and other estuaries, and in controlling the fate of land-derived organic matter in ocean margins (e.g. Hedges et al., 1997).

5. Summary

The behavior of particulate constituents relative to salt indicates that there were net landward fluxes of TSS, POC, and PON in portions of the water column along the main channel of Winyah Bay under the low river discharge regime encountered in this study. The direction of these local fluxes is controlled by the

residual circulation of the estuary as well as the effects of tidally-controlled resuspension. During the observed landward flux lower density particles with enhanced OC contents and elevated C/N ratios appear to be preferentially transported up the estuary. Overall, most of the suspended POM is predominantly derived from terrigenous C_3 plant sources with significant contributions from river and estuarine phytoplankton sources. Long-term estimates of transport and fate of POM require additional sampling during periods of high discharge as well as along cross-sectional transects over the shallow areas of the estuary. We expect that the behavior of sediments and POM will be distinct under these conditions than what was observed in this study.

Acknowledgements

This work was supported by the Environmental Protection Agency/EPSCoR grant No. R-82942401-O. Ship time on board the R/V Ferrel was provided by the National Ocean and Atmosphere Administration (NOAA) through the National Estuarine Research Reserve System (NERRS) program. The captain (Jim Meigs) and crew of the NOAA R/V Ferrel are thanked for their assistance. We would also like to acknowledge the assistance provided during data collection by Juana Montane, Natalie Monacci, Audrey Thompson, Sam Myers, and Benjamin Guttierez. Finally, we would like to thank the two anonymous reviewers whose comments helped improve this contribution.

References

Abril, G., Nogueira, M., Etcheber, H., Cabecadas, G., Lemaire, E., Brogueira, M.J., 2002. Behavior of organic carbon in nine contrasting European estuaries. Estuarine, Coastal and Shelf Science 54, 241–262.

Allen, G.P., Salomon, J.C., Bassoullet, P., Du-Penhoat, Y., De-Grandpre, C., 1980. Effects of tides on mixing and suspended sediment transport in macrotidal estuaries. Sedimentary Geology 26, 69–90.

Aller, R.C., 1998. Mobile deltaic and continental shelf muds as suboxic, fluidized bed reactors. Marine Chemistry 61, 143–155.

Aller, R.C., 1994. Bioturbation and remineralization of sedimentary organic matter – effects of redox oscillation. Chemical Geology 114, 331–345.

Blood, E.R., Vernberg, J.F., 1992. Characterization of Physical, Chemical and Biological Conditions and Trends in Winyah Bay and North Inlet Estuaries: 1970–1985, vol. 2. Winyah Bay and North Inlet estuaries. South Carolina Sea Grant Consortium. Charleston, South Carolina, 117 pp.

Canuel, E.A., 2001. Relations between river flow, primary production and fatty acid composition of particulate organic matter in San Francisco and Chesapeake Bays: a multivariate approach. Organic Geochemistry 32, 563–583.

Canuel, E.A., Cloern, J.E., Ringelberg, D.B., Guckert, J.B., Rau, G.H., 1995. Molecular and isotopic tracers used to examine sources of organic matter and its incorporation into the food webs of San Francisco Bay. Limnology and Oceanography 40, 67–81.

Chant, R.J., Stoner, A.W., 2001. Particle trapping in a stratified flood-dominated estuary. Journal of Marine Research 59, 29–51.

Cheng, R.T., Casulli, V., 1982. On Lagrangian residual currents with applications in South San Francisco Bay, California. Water Resources Research 18, 1652–1662.

Cifuentes, L.A., Eldridge, P.M., 1998. A mass- and isotope-balance model of DOC mixing in estuaries. Limnology and Oceanography 43, 1872–1882.

Cifuentes, L.A., Sharp, J.H., Fogel, M.L., 1988. Stable carbon and nitrogen isotope biogeochemistry in the Delaware Estuary. Limnology and Oceanography 33, 1102–1115.

Ertel, J.R., Alberts, J.J., Price, M.T., 1991. Transformation of riverine organic matter in estuaries. In: Hatcher, K.J. (Ed.), Proceedings of the 1991 Georgia Water Resources Conference, Institute of Natural Resources, University of Georgia, Athens, Georgia, pp. 309–312.

Fisher, T.R., Hagy, J.D., Rochelle-Newall, E., 1998. Dissolved and particulate organic carbon in Chesapeake Bay. Estuaries 21, 215–229.

Friedrichs, C.T., Wright, L.D., Hepworth, D.A., Kim, S.C., 2000. Bottom-boundary-layer processes associated with fine sediment accumulation in coastal seas and bays. Continental Shelf Research 20, 807–841.

Friedrichs, C.T., Armbrust, B.A., de Swart, H.E., 1998. Hydrodynamics and sediment dynamics of shallow, funnel-shaped tidal estuaries. In: Dronkers, J., Scheffers, M. (Eds.), Physics of Estuaries and Coastal Seas. Balkema Press, Rotterdam, The Netherlands, pp. 315–328.

Geyer, W.R., 1993. The importance of suppression of turbulence by stratification on the Estuarine Turbidity Maximum. Estuaries 16, 113–125.

Goñi, M.A., Teixeira, M.J., Perkey, D.W., 2003. Sources and distribution of organic matter in a river-dominated estuary (Winyah Bay, SC, USA). Estuarine, Coastal and Shelf Science 57, 1023–1048.

Goñi, M.A., Ruttenberg, K.C., Eglinton, T.I., 1998. A reassessment of the sources and importance of land-derived organic matter in surface sediments from the Gulf of Mexico. Geochimica et Cosmochimica Acta 62, 3055–3075.

Harvey, H.R., Mannino, A., 2001. The chemical composition and cycling of particulate and macromolecular dissolved organic matter and xenobiotics: bioavailability of pyrene and 2,2′,5,5′-tetrachlorobiphenyl to Daphnia magna. Chemosphere 38, 335–350.

Hedges, J.I., Keil, R.G., Benner, R., 1997. What happens to terrestrial organic matter in the ocean? Organic Geochemistry 27, 195–212.

Hedges, J.I., Clark, W.A., Quay, P.D., Richey, J.E., Devol, A.H., Santos, U.M., 1986. Composition and fluxes of particulate organic material in the Amazon River. Limnology and Oceanography 31, 717–738.

Hedges, J.K., Stern, J.H., 1984. Carbon and nitrogen determinations of carbonate-containing solids. Limnology and Oceanography 29, 657–663.

Hopkinson, C.S., Buffam, I., Hobbie, J., Vallino, J., Perdue, M., Eversmeyer, B., Prahl, F., Covert, J., Hodson, R.E., Moran, M.A., Smith, E., Baross, J., Crump, B., Findlay, S., Foreman, L., 1998. Terrestrial inputs of organic matter to coastal ecosystems: an intercomparison of chemical characteristics and bioavailability. Biogeochemistry 43, 211–234.

Jay, D.A., 1991. Estuarine salt conservation: a Lagrangian approach. Estuarine, Coastal and Shelf Science 32, 547–565.

Keil, R.G., Tsamakis, E., Bor Fuh, C., Giddings, J.C., Hedges, J.I., 1994. Mineralogical and textural controls on the organic composition of coastal marine sediments: hydrodynamic separation using SPLITT-fractionation. Geochimica et Cosmochimica Acta 58, 879–893.

Kim, Y.H., Voulgaris, G. Tidal and residual estuarine circulation in Winyah Bay, SC. Estuarine, Coastal and Shelf Science, submitted for publication.

Komada, T., Reimers, C.E., 2001. Resuspension-induced partitioning of organic carbon between solid and solution phases from a river–ocean transition. Marine Chemistry 76, 155–174.

Leithold, E.L., Blair, N.E., 2001. Watershed control on the carbon loading of marine sedimentary particles. Geochimica et Cosmochimica Acta 65, 2231–2240.

Longuet-Higgins, M.S., 1989. On the transport of mass by time-varying ocean currents. Deep-Sea Research 16, 431–447.

Masiello, C.A., Druffel, E.R.M., 2001. Carbon isotope geochemistry of the Santa Clara River. Global Biogeochemical Cycles 15, 407–416.

Müller, P.J., 1977. C/N ratios in Pacific deep-sea sediments: effect of inorganic ammonium and organic nitrogen compounds sorbed by clays. Geochimica et Cosmochimica Acta 41, 765–776.

Murrell, M.C., Hollibaugh, J.T., 2000. Distribution and composition of dissolved and particulate organic carbon in northern San Francisco Bay during low flow conditions. Estuarine, Coastal and Shelf Science 51, 75–90.

Pritchard, D.W., 1967. Observation of circulation in coastal plain estuaries. American Association Advanced Science 83, Washington, DC, 3–5.

Ramsey, A.L., 2000. Physical processes controlling sediment transport in Winyah Bay, South Carolina. MS thesis, Boston College, Boston, MA, 134 pp.

Raymond, P.A., Bauer, J.E., 2000. Bacterial consumption of DOC during transport through a temperate estuary. Aquatic Microbial Ecology 22, 1–12.

Ruttenberg, K.C., Goni, M.A., 1997. Phosphorus distribution, C:N:P ratios, and $\delta^{13}C_{OC}$ in arctic, temperate, and tropical coastal sediments: tools for characterizing bulk sedimentary organic matter. Marine Geology 139, 123–145.

Schubel, J.R., Pritchard, D.W., 1972. The estuarine environment, part 1. Journal of Geological Education 20, 60–68.

Schubel, J.R., 1968. Turbidity maximum of the northern Chesapeake Bay. Science 161, 1013–1015.

Shi, W., Sun, M.Y., Molina, M., Hodson, R.E., 2001. Variability in the distribution of lipid biomarkers and their molecular isotopic composition in Altaqmaha estuarine sediments: implications for the relative contribution of organic matter from various sources. Organic Geochemistry 32, 453–467.

Taylor, J.R., 1982. An introduction to error analysis: the study of uncertainties in physical measurements. University Science Books, Mill Valley California.

Teixeira, M.J., 2000. Characterization, distribution and association of natural organic matter and polycyclic aromatic hydrocarbons in Winyah Bay, South Carolina. MS thesis, University of South Carolina, Columbia, SC, 202 pp.

USACOE, 1997. Dredged material management plan, preliminary assessment – Georgetown SC.

Yunker, M.B., Macdonald, R.W., Veltkamp, D.J., Cretyney, W.J., 1995. Terrestrial and marine biomarkers in a seasonally ice-covered arctic estuary – integration of multivariate and biomarker approaches. Marine Chemistry 19, 1–50.

Zhang, J., Liu, S.M., Xu, H., Yu, Z.G., Lai, S.Q., Zhang, H., Geng, G.Y., Chen, J.F., 1998. Riverine sources and estuarine fates of particulate organic carbon from North China in late summer. Estuarine, Coastal and Shelf Science 46, 439–448.

Zimmerman, J.T.F., 1979. On the Euler–Lagrange transformation and the Stokes' drift in the presence of oscillatory and residual currents. Deep-Sea Research 26A, 505–520.